ISSN 0010-9525, Cosmic Research, 2017, Vol. 55, No. 2, pp. 88–100. © Pleiades Publishing, Ltd., 2017.
Original Russian Text © Zh.V. Dashkevich, V.E. Ivanov, T.I. Sergienko, B.V. Kozelov, 2017, published in Kosmicheskie Issledovaniya, 2017, Vol. 55, No. 2, pp. 94–106.

Physicochemical Model of the Auroral Ionosphere

Zh. V. Dashkevich[a], *, V. E. Ivanov[a], T. I. Sergienko[b], and B. V. Kozelov[a]

[a] *Polar Geophysical Institute, Russian Academy of Sciences, Apatity, 184200 Russia*
[b] *Swedish Institute of Space Physics, Kiruna, Sweden*
**email: zhanna@pgia.ru*

Received March 13, 2016

Abstract—A physicochemical model of excited polar ionosphere has been presented. The model makes it possible to calculate vertical profiles of concentrations of the following excited and ionized constituents: O_2^+, N_2^+, $O^+(^4S)$, $O^+(^2D)$, $O^+(^2P)$, $O(^1D)$, $O(^1S)$, $N(^4S)$, $N(^2D)$, $N(^2P)$, NO, NO^+, N^+, $N_2\left(A^3\Sigma_u^+\right)$, $N_2(B^3\Pi_g)$, $N_2(W^3\Delta_u)$, and $N_2\left(B'^3\Sigma_u^-\right)$ and the electron concentration during electron precipitations. The energy spectrum of the electrons at the upper boundary of the ionosphere and concentrations of neutral constituents are the input parameters of the model. A model has been compiled based on available publications and includes 56 physicochemical reactions that influence concentrations of the aforementioned constituents in the polar ionosphere. The method of calculating vertical profiles of the excitation rates of atmospheric gases and proper allowance for the electron-vibrational kinetics in the processes of exciting the triplet states of N_2 are specific features of the presented model. The ionospheric model has been approbated using the results of the coordinated rocket–satellite experiment. The agreement between the modeling results and experimental data best for the time being is achieved.

DOI: 10.1134/S0010952517020022

1. INTRODUCTION

Modeling the processes that occur in the ionosphere during the precipitation of auroral electrons is an important element in studying and understanding the physics of the disturbed polar ionosphere. Models of that class should describe both the processes of the excitation of electronically vibrational states of the ionospheric plasma constituents by a direct electronic impact and the subsequent redistribution of the revealed energy due to the initiated chemical reactions. Parameters of the precipitating electron flux, neutral atmosphere model, and the set of chemical reactions with the corresponding rate constants are the main input parameters of these models. A nonstationary model of the ionosphere disturbed by electron flux, including 29 chemical reactions, was presented in [1, 2]. In the scope of that model, the time dynamics of the ionospheric ion composition and the intensity of the main auroral emissions were studied. Later, the testing of the model was performed using the data of the coordinated rocket–satellite experiment described in [3, 4]. During this experiment, the following parameters were measured onboard the rocket launched into the region of an auroral arc and onboard a satellite flying in the neighborhood of the aurora: the energy spectrum of the electrons flux; concentrations of atmospheric gases N_2, O_2, and O within the height interval of 160–240 km; vertical profiles of concentrations of N_2^+, O_2^+, O^+, and NO^+ ions; and vertical profiles of the intensity of the emissions of 557.7 and 630.0 nm of atomic oxygen, 391.4 nm of the first negative system of the N_2^+ bands, 337.1 nm of the second positive system of N_2 bands, and 320.0 nm of the Vegard–Kaplan system of N_2 bands. According to the test results, the satisfactory agreement of the modeling results with the experimental data could only be seen in [3, 4] for the intensities of the 391.4- and 557.7-nm emissions. For the ion composition, the calculated values substantially exceed the measured values, on average by a factor of 2.5 for O_2^+ ion and on average by a factor of 2 for the O^+ ion within the entire height interval. An increase in the difference between the measured and calculated concentrations of NO^+ ions is observed with a height decrease from 170 to 110 km. A nonstationary model of the auroral ionosphere including odd nitrogen NO, $N(^2D)$, and $N(^4S)$, was also used in [5] to model the ion composition measured in the coordinate rocket–satellite experiment described in [3]. Satisfying agreement between the measured and calculated values of O_2^+, O^+, and NO^+ concentrations was obtained in [5] at all altitudes. However, on average, the calculated concentrations of

N_2^+ exceeded the measured concentrations by a factor of three.

A nonstationary-in-time model of disturbed polar ionosphere, which includes 56 physicochemical processes that participate in the redistribution of the energy revealed into the medium, is presented in this paper. The following features are specific to the given model:

(1) a functional that makes it possible to calculate vertical profiles of the excitation rates of atmospheric gases N_2, O_2, and O at various electronically vibrational states under an arbitrarily taken differential flux of precipitating electrons;

2) an algorithm for recovering the energy spectrum of the precipitating electron flux using the vertical profile of the band luminosity, the emission of which corresponds to the permitted transitions in the given paper of the bands of the first negative system of N_2^+;

(3) a method for calculating the population of vibrational levels of the triplet electron states of N_2.

The latter is especially important for the $A^3\sum_u^+$, term, which plays a dominant role in the excitation of the ^1S state of atomic oxygen, which is a source of a 557.7-nm emission.

2. MODEL

1. Auroral electrons that are precipitated into the polar ionosphere lose their energy at collisions to atoms and molecules of atmospheric gases and initiate physicochemical processes, including the excitation and ionization of these gases. As a result, a complicated complex of chemical reactions that determine the composition of the disturbed ionosphere is originated. At the high-latitude ionosphere at heights of the *E* and *F*1 regions (~90–160 km) where the transport processes of low-energy constituents could be neglected, the numerical modeling of these processes is reduced to solving a system of nonstationary one-dimensional continuity equations of the type

$$\frac{dN_{Yk}(h,t)}{dt} = Q_{Yk}(h,t) + Q^*_{Yk}(h,t) - L_{Yk}(h,t), \quad (1)$$

where $N_{Yk}(h, t)$ is the concentration of the *Y* component of the atmospheric gas excited to the *k*th state, $Q_{Yk}(h, t)$ is the rate of formation of the *Yk* state due to a direct impact, $Q^*_{Yk}(h, t)$ is the rate of formation of the *Yk* state in chemical reactions, $L_{Yk}(h, t)$ is the rate of quenching of the *Yk* state in chemical reactions and emitting transitions, *h* is the height over the Earth's surface, and *t* is the precipitations duration.

The method of calculation of vertical profiles of the rates of excitation and ionization of atmospheric gases $Q_{Yk}(h, t)$ by precipitating electron flux is a distinctive feature of the presented model. This method is based on a functional proposed in [6–8] which makes it possible to relate analytically the vertical profiles of the excited components of the atmosphere to the energy spectrum of the precipitating electrons *F*(*E*). Under a condition that the precipitating electron flux does not change with time, this relation will be as follows:

$$Q_{Yk}(h) = P_Y(h)\rho(h) \times \frac{1}{\varepsilon_{Yk}}\int_E \frac{E\,F(E)[1-T_E(E)]}{R(E)}\lambda(E,\chi)\,dE, \quad (2)$$

where $P_Y(h)$ is the portion of the energy spent to excitation of the atmospheric gas of the *Y* type, $\rho(h)$ is the atmospheric density, ε_{Yk} is the energy price of excitation of the *k*th state of the atmospheric gas of the *Y* type, *F*(*E*) is the energy spectrum of precipitating electrons, $T_E(E)$ is the value of the albedo-flux over the energy, *R*(*E*) is the integral free path, $\lambda(E, \chi)$ is a dimensionless function of energy dissipation, and χ is the depth of penetration into the atmosphere normalized to the integral free path. The $T_E(E)$, *R*(*E*), and $\lambda(E, \chi)$ dependences obtained in [6–8] were used in the calculations in this paper.

The rate of excitation of the *k*th state of the *Y*th constituent of the atmospheric gases in collisional reactions is determined as

$$Q^*_{Yk}(h,t) = \sum_X \sum_Z N_X(h,t)\,N_Z(h,t)\,k_{XZ}, \quad (3)$$

where $N_X(h, t)$ and $N_Z(h, t)$ are the concentrations of gases of the *X* and Z types and k_{XZ} is the rate constant of the reaction.

The losses $L_{Yk}(h, t)$ are compiled of the losses in collisional reactions of quenching and emitting transitions and are determined as

$$L_{Yk}(h,t) = \sum_X N_{Yk}(h,t)\,N_X(h,t)\,k_{YX} + \sum_i A^{Yk}_{Yi} N_{Yk}(h,t), \quad (4)$$

where $N_{Yk}(h, t)$ and $N_X(h, t)$ are the concentrations of the gas in the *Yk* state and the gas of the *X* type, k_{YX} is the rate constant of the deactivation reaction, and A^{Yk}_{Yi} is the probability of spontaneous emission of the *Yk* state with a transition to *Yi*.

Thus, in the model presented here, the concentration of ionospheric constituents N_2^+, O_2^+, $O^+(^4S)$, $O^+(^2D)$, $O^+(^2P)$, $O(^1D)$, $O(^1S)$, $N(^4S)$, $N(^2D)$, $N(^2P)$, NO, NO^+, N^+, $N_2(A^3)$, and the electron concentration n_e are connected by 56 chemical reactions. The reactions used in the model and corresponding rate constants are shown in table.

Reactions and their rate constants used in the model

No.	Reaction	Reaction rate constant, $cm^3\ s^{-1}$	References
1	$N_2^+ + O_2 \rightarrow N_2 + O_2^+$	$k_1 = 5\times10^{-11}\times(300/T_i)^{0.8}$	[9]
2	$N_2^+ + O \rightarrow N_2 + O^+(^4S)$	$k_2 = 9.8\times10^{-12}\times(300/T_i)^{0.23}$	[10]
3	$N_2^+ + O \rightarrow NO^+ + N(^2D)$	$k_3 = 1.4\times10^{-10}\times(300/T_i)^{0.44} - k_2$ $f_{2_D} = 0.9$	[10]
4	$N_2^+ + NO \rightarrow N_2 + NO^+$	$k_4 = 3.3\times10^{-10}$	[11]
5	$N_2^+ + e \rightarrow N(^4S) + N(^2D)$	$k_5 = 3.5\times10^{-7}\times(300/T_e)^{0.5}$ $f_{4_S} = 0.1, f_{2_D} = 1.9$	[12] [13]
6	$O_2^+ + e \rightarrow O(^1S) + O(^1D)$	$k_6 = 1.9\times10^{-7}\times(300/T_e)^{0.5}$ $f_{1_D} = 1.2, f_{1_S} = 0.1$	[12] [14]
7	$O_2^+ + N(^4S) \rightarrow NO^+ + O(^1S)$	$k_7 = 1.2\times10^{-10}$ $f_{1_S} = 0.2$	[15] [16]
8	$O_2^+ + NO \rightarrow NO^+ + O_2$	$k_8 = 4.4\times10^{-10}$	[17]
9	$O_2^+ + N(^2D) \rightarrow NO^+ + O$	$k_9 = 1.8\times10^{-10}$	[18]
10	$O^+(^4S) + N_2 \rightarrow NO^+ + N(^4S)$	$k_{10} = 1.533\times10^{-12} - 5.92\times10^{-13}\times(T_i/300) + 8.6\times10^{-14}\times(T_i/300)^2$	[19]
11	$O^+(^4S) + O_2 \rightarrow O_2^+ + O$	$k_{11} = 2.82\times10^{-11} - 7.74\times10^{-12}\times(T_i/300) + 1.073\times(T_i/300)^2 - 5.17\times10^{-14}\times (T_i/300)^3 + 9.65\times10^{-16}\times(T_i/300)^4$	[19]
12	$O^+(^4S) + NO \rightarrow NO^+ + O$	$k_{12} = 8.36\times10^{-13} - 2.02\times10^{-13}\times(T_i/300) + 6.95(T_i/300)^2$	[19]
13	$O^+(^2D) + N_2 \rightarrow N_2^+ + O$	$k_{13} = 7.2\times10^{-10}$	[20]
14	$O^+(^2D) + N_2 \rightarrow NO^+ + N(^4S)$	$k_{14} = 8\times10^{-11}$	[20]
15	$O^+(^2D) + O_2 \rightarrow O_2^+ + O$	$k_{15} = 6.3\times10^{-10}$	[20]
16	$O^+(^2D) + O_2 \rightarrow O^+(^4S) + O_2$	$k_{16} = 7\times10^{-11}$	[20]
17	$O^+(^2D) + O \rightarrow O^+(^4S) + O$	$k_{17} = 1\times10^{-11}$	[21]
18	$O^+(^2D) + e \rightarrow O^+(^4S) + e$	$k_{18} = 6.6\times10^{-8}\times(300/T_e)^{0.5}$	[22]
19	$O^+(^2D) \rightarrow O^+(^4S) + h\nu$	$A_{19} = 0.97\times10^{-4}$	[23]
20	$O^+(^2P) + N_2 \rightarrow O^+(^4S) + N_2$	$k_{20} = 4\times10^{-10}$	[24]
21	$O^+(^2P) + N_2 \rightarrow N_2^+ + O$	$k_{21} = 5\times10^{-11}$	[24]
22	$O^+(^2P) + O \rightarrow O^+(^4S) + O$	$k_{22} = 5\times10^{-11}$	[25]
23	$O^+(^2P) + O_2 \rightarrow O_2^+ + O$	$k_{23} = 4.8\times10^{-10}$	[26]
24	$O^+(^2P) \rightarrow O^+(^2D) + h\nu$	$A_{24} = 0.171$	[27]
25	$O^+(^2P) \rightarrow O^+(^4S) + h\nu$	$A_{25} = 0.048$	[28]
26	$O^+(^2P) + e \rightarrow O^+(^2D) + e$	$k_{26} = 1.4\times10^{-7}\times(300/T_e)^{0.5}$	[29]
27	$O^+(^2P) + e \rightarrow O^+(^4S) + e$	$k_{27} = 4.4\times10^{-8}\times(300/T_e)^{0.5}$	[29]
28	$O(^1D) + N_2 \rightarrow O + N_2$	$k_{28} = 2\times10^{-11}\exp(107.8/T_n)$	[30]
29	$O(^1D) + O_2 \rightarrow O + O_2$	$k_{29} = 2.9\times10^{-11}\exp(67.5/T_n)$	[30]

Table. (Contd.)

No.	Reaction	Reaction rate constant, $cm^3\ s^{-1}$	References
30	$O(^1D) + O \rightarrow O + O$	$k_{30} = 8\times10^{-12}$	[31]
31	$O(^1D) \rightarrow O + h\nu$	$A_{31} = 9.3\times10^{-3}$	[32]
32	$O(^1D) + e \rightarrow O + e$	$k_{32} = 1.6\times10^{-12}T_e^{0.91}$	[33]
33	$O(^1S) + O \rightarrow O + O$	$k_{33} = 2\times10^{-14}$	[34]
34	$O(^1S) \rightarrow O(^1D) + h\nu$	$A_{34} = 1.06$	[23]
35	$O(^1S) \rightarrow O + h\nu$	$A_{35} = 0.045$	[23]
36	$O(^1S) + O_2 \rightarrow O + O_2$	$k_{36} = 4\times10^{-12}\exp(-860/T_n)$	[35]
37	$O(^1S) + NO \rightarrow O + NO$	$k_{37} = 5.5\times10^{-13}$	[36]
38	$N(^4S) + O_2 \rightarrow NO + O$	$k_{38} = 4.4\times10^{-12}\exp(-3600/T_n)$	[37]
39	$N(^4S) + NO \rightarrow N_2 + O$	$k_{39} = 3.4\times10^{-11}$	[38]
40	$N(^2D) + O_2 \rightarrow NO + O(^3P,^1D)$	$k_{40} = 6\times10^{-12}$ $f_{1_D} = 0.1$	[39] [40]
41	$N(^2D) + O \rightarrow N(^4S) + O(^3P,^1D)$	$k_{41} = 6.9\times10^{-13}$ $f_{1_D} = 0.1$	[41]
42	$N(^2D) + NO \rightarrow N_2 + O$	$k_{42} = 6.7\times10^{-11}$	[38]
43	$N(^2D) + NO \rightarrow N(^4S) + NO$	$k_{43} = 6.3\times10^{-11}$	[42]
44	$N(^2D) + e \rightarrow N(^4S) + e$	$k_{44} = 5.5\times10^{-10}\times(T_e/300)^{0.5}$	[43]
45	$N(^2D) \rightarrow N(^4S) + h\nu$	$A_{45} = 1.07\times10^{-5}$	[27]
46	$N(^2P) + O_2 \rightarrow NO + O(^1S,^1D,^3P$	$k_{46} = 3.5\times10^{-12}$ $f_{1_S1_D3_P} = 0.33$	[38]
47	$N(^2P) + O \rightarrow N(^2D) + O$	$k_{47} = 1\times10^{-11}$	[44]
48	$N(^2P) \rightarrow N(^2D) + h\nu$	$A_{48} = 5.4\times10^{-3}$	[45]
49	$N(^2P) \rightarrow N(^4S) + h\nu$	$A_{49} = 7.9\times10^{-2}$	[45]
50	$N(^2P) + NO \rightarrow N_2 + O$	$k_{50} = 2.9\times10^{-11}$	[46]
51	$NO^+ + e \rightarrow O + N(^4S,^2D)$	$k_{51} = 2.3\times10^{-7}\times(300/T_e)^{0.5}$ $f_{4_S} = 0.24, f_{2_D} = 0.76$	[12] [47]
52	$N^+ + O_2 \rightarrow O_2^+ + N(^4S,^2D)$	$k_{52} = 3\times10^{-10}$ $f_{4_S} = 0.8, f_{2_D} = 0.2$	[48]
53	$N^+ + O_2 \rightarrow NO^+ + O(^1D,^1S)$	$k_{53} = 2.6\times10^{-10}$ $f_{1_D} = 0.7, f_{1_S} = 0.01$	[48]
54	$N^+ + O_2 \rightarrow O^+(^4S) + NO$	$k_{54} = 4\times10^{-11}$	[48]
55	$N^+ + O \rightarrow O^+(^4S) + N(^4S)$	$k_{55} = 1\times10^{-12}$	[49]
56	$N_2(A^3\Sigma_u^+) + O \rightarrow N_2 + O(^1S)$	$k_{56} = (2.8 + 0.886\lg v)\times10^{-11}$ $f_{1_S} = 0.55, 0.12, 0.16, 0.26, 0.13, 0.16, 0.23, 0.16, 0.12$	[50]

f_{1_S} is a yield $O(^1S)$ in the indicated reaction.

2. The triplet states of the molecular nitrogen $N_2\left(A^3\sum_u^+\right)$, $N_2(B^3\Pi_g)$, and $N_2(C^3\Pi_u)$ are sources of emissions of the Vegard–Kaplan system bands, first positive system bands, and second positive system bands, respectively, which are reliably registered in auroras. Moreover, the triplet state $N_2\left(A^3\sum_u^+\right)$ participates in the formation of excited atomic oxygen $O(^1S)$, which is a source of the auroral green line, while the rate of formation of excited oxygen depends on the vibrational number of the triplet level $A^3\sum_u^+$.

The description of the electronically vibrational kinetics in formation of the triplet states of N_2 is based on allowance for the following processes:

excitation by direct electron impact from the main undisturbed level of molecular nitrogen

$$N_2\left(X^1\Sigma_g^+, v'\right) + e^* \rightarrow N_2\left(L_i, v''\right) + e;$$

spontaneous transitions between the triplet levels of molecular nitrogen

$$N_2\left(L_i, v\right) \leftrightarrow N_2\left(L_j, v''\right) + h\nu;$$

energy transfer between the triplet states via collisional reactions of excited molecules

$$N_2\left(L_i, v\right) + N_2\left(X^1\Sigma_g^+, v'' = 0\right) \rightarrow N_2\left(L_j, v'\right) + N_2\left(X^1\Sigma_g^+, v'' \geq 0\right);$$

energy redistribution between vibrational levels of the triplet state

$$N_2\left(L_i, v\right) + N_2\left(X^1\Sigma_g^+, v'' = 0\right) \rightarrow N_2(L_i, v') + N_2\left(X^1\Sigma_g^+, v'' \geq 0\right);$$

emitting spontaneous transitions

$$N_2(L_i, v) \rightarrow N_2\left(X^1\Sigma_g^+ \vee L_j\right) + h\nu;$$

inelastic collisional reactions of quenching with the main atmospheric gases O, N_2, and O_2

$$N_2(L_i, v) + Z \rightarrow N_2\left(X^1\Sigma_g^+\right) + Z^*.$$

Here L_i and L_j are the triplet terms and v is the vibrational quantum number.

The vibrational kinetics of triplet states is based on the model described in [51]. In addition to model [51], in this paper, we take into account the redistribution of the energy between the vibrational levels of the triplet state.

The calculation of the rate of formation for each vibrational level of the triplet state is reduced to solving the system of basis equations. Taking into account the small radiative lifetime of the triplet terms, the balance equations may be written in the photochemical equilibrium approximation

$$\begin{aligned} Q_{L_i} q_{v'}^{L_i} + \sum_{v'} N_{v'}^{L_i} A_{v'v}^{L_j L_i} + \sum_{v', L_j} N_{v'}^{L_j}[N_2] k_{v'}^{L_j L_i} \\ + \sum_{v'} N_{v'}^{L_i}[N_2] k_{v'v}^{L_i L_i} = \sum_{v'} N_{v'}^{L_i} A_{vv'}^{L_i L_j} \\ + \sum_{v', L_i} N_{v'}^{L_i} A_{vv'}^{L_j L_i} + \sum_{v} N_{v'}^{L_i}[N_2] k_{v'v}^{L_i L_i} \\ + \sum_{v'} N_{v'}^{L_i}[N_2] k_{v'v}^{L_i L_i} + \sum_{Z} N_v^{L_i}[Z] k_v^{L_i Z}, \end{aligned} \quad (5)$$

where $N_v^{L_i}$ is the population of the vibrational level v of the term L_i; Q_{L_i} is the formation rate of the triplet term L_i; $q_v^{L_i}$ are the Franck–Condon factors; $A_{vv'}^{L_i L_j}$ are the Einstein coefficients for the transition from the L_i, v level to the level L_j, v'; $k_{vv'}^{L_i L_j}$ is the rate of the collisional reaction with energy transfer from the L_i, v level to the level L_j, v'; $k_v^{L_i Z}$ is the quenching rate of the level L_i, v by the atmospheric gas Z; and [Z] is the concentration of this gas Z.

In order to determine the vibrational population of the N_2 triplet levels, a linear system of 73 balance equations was compiled for 22 vibrational levels of the $A^3\sum_u^+$ term, 13 vibrational levels of the $B^3\Pi_g$ term (this term predissociates beginning from the thirteenth vibrational level), 19 vibrational levels of the $W^3\Delta_u$ term, 14 vibrational levels of the $B'^3\sum_u^-$ term, and 5 vibrational levels of the $C^3\Pi_u$ term. The number of levels was chosen based on the expediency principle taking into account the mutual location of the vibration triplets. The rates of the formation of electron terms Q_L were calculated analagously to (2). The Franck–Condon factors and Einstein coefficients, energetic prices, and rates of collisional reactions with the transfer and redistribution of energy $k_{vv'}^{LL'}$ were taken from [52], [8], and [53], respectively. The rates of quenching of the triplet levels by the atmospheric gases O, O_2, and N_2 were taken from [51, 54]. Figures 1 and 2 show the calculated distributions of the population of vibrational levels of the $A^3\sum_u^+$ and $C^3\Pi_u$ triplets. A comparison of the calculated populations with the theoretical results from [52] and experimental estimates from [55, 56] show a satisfactory agreement. Figure 3 shows the distributions of populations of vibrational levels of the $A^3\sum_u^+$ triplet calculated for different height levels. It can be seen that, unlike the

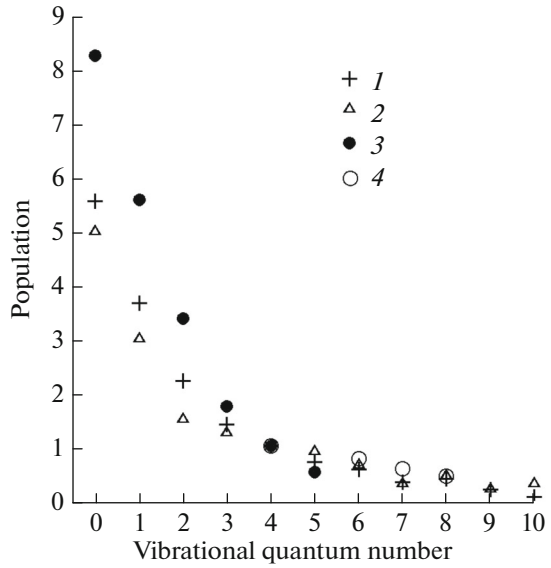

Fig. 1. Distribution of the vibrational population of the $A^3\Sigma_u^+$ term: (*1*) calculation for a height of 100 km, (*2*) calculation from [53], (*3*) experimental results from [55], and (*4*) experimental results from [56].

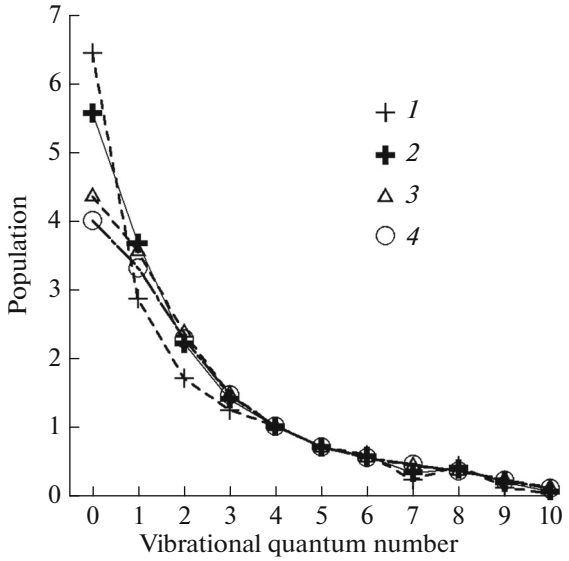

Fig. 3. Distribution of the vibrational population of the $A^3\Sigma_u^+$ term at various heights: (*1*) 85 km, (*2*) 100 km, (*3*) 150 km, and (*4*) 170 km

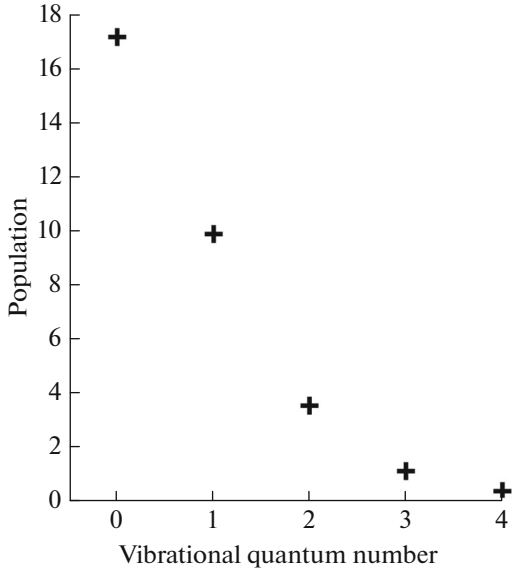

Fig. 2. Distribution of the vibrational population of the electron level $C^3\Pi_u$ of molecular nitrogen.

$C^3\Pi_u$ level, the population of vibrational levels of $A^3\Sigma_u^+$ depends on height, with the lower levels ($v < 4$) being the most sensitive to its change.

The model presented in this paper makes it possible to calculate concentrations of the following constituents: N_2^+, O_2^+, $O^+(^4S)$, $O^+(^2D)$, $O^+(^2P)$, $O(^1D)$, $O(^1S)$, $N(^4S)$, $N(^2D)$, $N(^2P)$, NO, NO^+, N^+, $N_2(A^3)$, $N_2\left(A^3\Sigma_u^+\right)$, $N_2(B^3\Pi_g)$, $N_2(W^3\Delta_u)$, $N_2\left(B'^3\Sigma_u^-\right)$, $N_2(C^3\Pi_u)$, and electrons in the auroral polar ionosphere. The energy spectrum of the precipitating electrons and the neutral atmosphere model are the input parameters of the model. The model is applicable to the *E* and lower *F* ionospheric regions because it does not take into account the effects of the mass transport of excited components of the ionosphere.

3. RECONSTRUCTION OF THE ENERGY SPECTRUM OF PRECIPITATING ELECTRONS

The energy spectrum of the precipitating electrons flux is one of the main input parameters in auroral ionosphere models. The shape of the energy spectrum and value of the precipitating electrons flux could be reconstructed from the measured vertical profiles of the auroral emissions intensity. Emissions of short-living excited ionospheric species that do not participate in ionospheric chemical reactions best fit the reconstruction of the electron spectrum. First of all, these are the emissions of the first negative system of bands of molecular nitrogen ion 1NG occurring due to the transition $N_2^+\left(B^2\Sigma_u^+ \rightarrow X^2\Sigma_g^+\right)$. Bands 391.4, 427.8, and 470.9 nm, which correspond to transitions from the vibrational levels $v' = 0$ of the $B^2\Sigma_u^+$ term to the vibrational level $v'' = 0$, 1, and 2 of the $X^2\Sigma_g^+$ term, respectively, are the most intense and reliably detected in auroras.

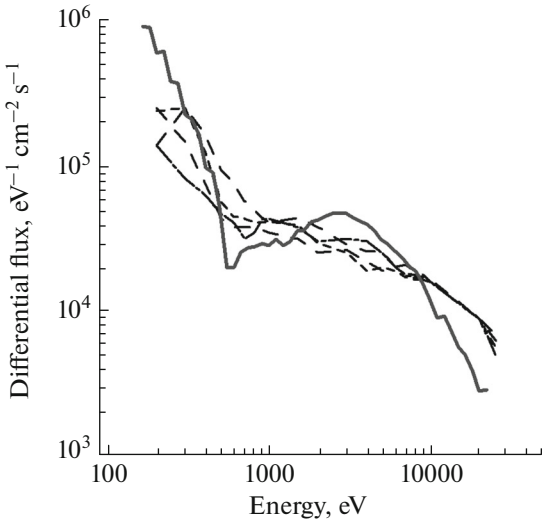

Fig. 4. Energy spectrum of precipitating electrons: solid semi-thick curve shows the reconstructed spectrum, dashed curves show energy spectrum measured on board the satellite [1].

The intensity of the 1NG band that corresponds to the transition $N_2^+\left(B^2\sum_u^+, v' \to X^2\sum_g^+, v''\right)$ is determined by the expression

$$I = A_{v'v''}\left[N_2^+\left(B^2\sum_u^+, v'\right)\right], \quad (6)$$

where I is the intensity of the band in the photon cm^{-3} s^{-1} units, $A_{v'v''}$ are the Einstein coefficients, and $\left[N_2^+\left(B^2\sum_u^+, v'\right)\right]$ is the concentration of N_2^+ in the $\left(B^2\sum_u^+, v'\right)$ state.

The concentration $\left[N_2^+\left(B^2\sum_u^+, v'\right)\right]$ is found by solving the balance equation of continuity (1). Taking into account the short lifetime of the $B^2\sum_u^+$ term ($\sim 10^{-7}$ s), it is possible to neglect the collisional deactivation of that state and to assume that it is completely quenched due to spontaneous transitions to the $X^2\sum_g^+$ term. Then, its concentration under the conditions of a stationary-in-time precipitating electron flux will be determined by the following equation:

$$0 = Q_{v'} - [N_2^+B^2\Sigma_u^+, v']\sum_{v'} A_{v'v''}. \quad (7)$$

Taking into account (6) and (7), we obtain

$$I = \frac{A_{v'v''}}{\sum_{v''} A_{v'v''}} Q_{v'}. \quad (8)$$

On the other hand, if any measured vertical profile of the intensity $I(h)$ is known, then generalizing the functional $Q_{v'}$ of formulae (2), expression (8) could be considered as an integral equation relative to the $F(E)$ function:

$$I(h) = B\int_E K(h,E)F(E)dE, \quad (9)$$

$$B = \frac{A_{v'v''}}{\sum_{v''} A_{v'v''}} P_{N_2}(h)\rho(h)\frac{q_{v'}}{\varepsilon_i};$$

$$K(h,E) = \frac{E\,(1 - T_E(E))}{R(E)}\lambda(E,\chi), \quad (10)$$

where $P_{N_2}(h)$ is the portion of the energy spent to excitation of N_2, q_v, are the Franck–Condon factors that correspond to the transitions from the ground state $N_2(X^2\sum_g^+, v'' = 0)$ to the excited levels $N_2^+\left(B^2\sum_u^+, v'\right)$, and ε_i is the energy price of the $B^2\sum_u^+$ level of the molecular nitrogen ion. The energy dissipation function $\lambda(E, \chi)$, integral free paths $R(E)$, value of the albedo-flux $T(E)$, and the energy price ε obtained in [6–8] were used in the calculations. The Einstein coefficients $A_{v'v''}$ and Franck–Condon factors q_v, were taken from [51].

We present the integral in formula (9) as the sum via the trapezium formula

$$I(h) = B\left\{\frac{K(h,E_1)F_1\Delta E_1}{2} + \left[\sum_{k=2}^{n-1}\frac{K(h,E_k)F_k(\Delta E_k + \Delta E_{k-1})}{2}\right] + \frac{K(h,E_n)F_n\Delta E_n}{2}\right\}, \quad (11)$$

where n is the number of points in the vertical profile of the emission intensity measured experimentally.

After introducing additional limitations that F_k should be positive, whereas the sought for $F(E)$ should be fairly smooth function of the energy, we come to the problem on minimization of the following functional:

$$L = \sum_i^n (I(h_i) - I_i)^2 + \sum_{k=2}^n (F_k - F_{k-1})^2. \quad (12)$$

The energy spectrum of precipitating electrons was reconstructed for a height of 500 km using the measured vertical profile of the intensity of the 391.4 nm emission intensity obtained in the experiment [4]. At the same time, the functional (12) was minimized using the gearing method. The solid curve in Fig. 4 shows the energy spectrum of the precipitating electrons reconstructed using the algorithm proposed above. The mean energy of the reconstructed spectrum is 8.5 keV at the flux of 10.5 erg cm^{-2} s^{-1}. Dashed

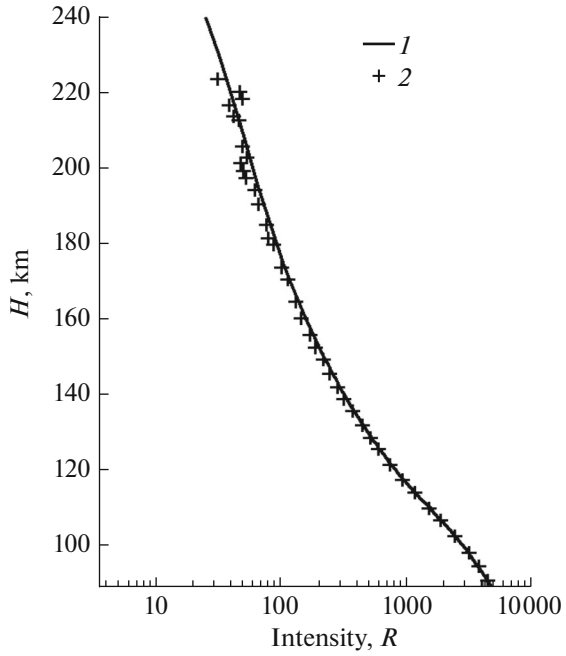

Fig. 5. Vertical profile of the intensity of the λ391.4 nm emission: (*1*) calculated using the reconstructed spectrum of precipitating electrons and (*2*) measured on board the rocket [4].

curves in Fig. 4 correspond to three sequent measurements conducted on board the satellite during the experiment [3]. It can be seen that the experimental and calculated spectra does not contradict each other. On the other hand, it should be taken into account that, during the measurements, the satellite was located at a distance of 800–500 km from the rocket and the energy spectra of electrons measured by the satellite could differ slightly from the spectra directly over the rocket flight region. That is why, subsequently, during modeling, the processes that occur in the disturbed ionosphere during electron precipitation, we will use the reconstructed precipitating electron flux that adequately describe the vertical profile of the 391.4 nm emission intensity. It is demonstrated in Fig. 5 where the comparison of the vertical profile of the 391.4 nm emission intensity measured in the experiment and calculated in accordance with (6) using the reconstructed energy spectrum of precipitating electrons is shown.

4. MODELING RESULTS

The results of the coordinated rocket–satellite experiment [3], in which the energy spectrum of auroral electrons, concentrations of the atmospheric gases N_2, O_2, and O within the height range of 160–240 km, vertical profiles of the concentrations of N_2^+, O_2^+, O^+, and NO^+ ions, vertical profiles of the intensities of emissions of the 557.7 and 630.0 nm of atomic oxygen, 391.4 nm of the first negative system of N_2^+, bands, 337.1 nm of the second positive system of N_2 bands, and 320.0 nm of the Vegard–Kaplan bands system were used to test the model. A detailed description of the experiment is presented in [3, 4]. It should be

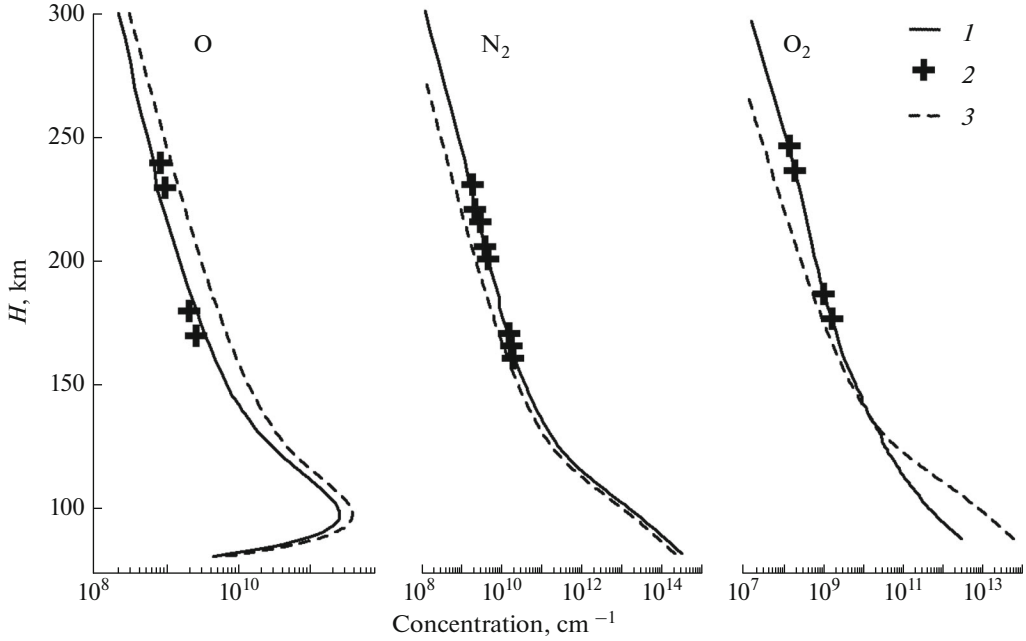

Fig. 6. Vertical profiles of the concentrations of atmospheric gases N_2, O_2, and O: (*1*) profile used in the model calculations, (*2*) experimental data [4], and (*3*) MSIS-90 [57].

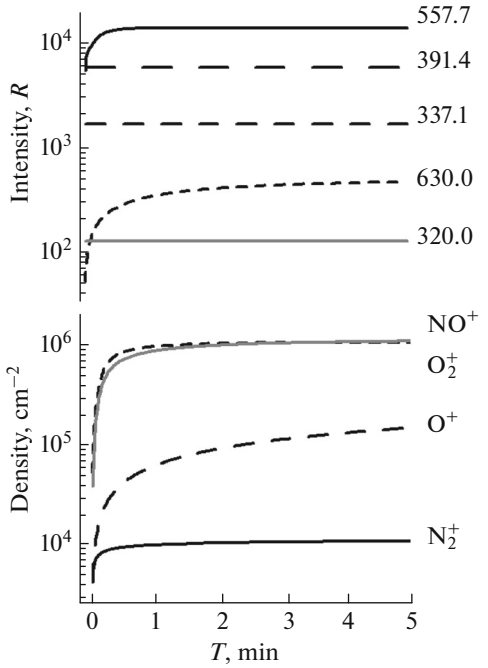

Fig. 7. Time dynamics of the concentrations of N_2^+,O_2^+, O^+, and NO^+ ions and emission intensities of 391.4-, 320.0-, 337.1-, 557.7-, and 630.0-nm lines.

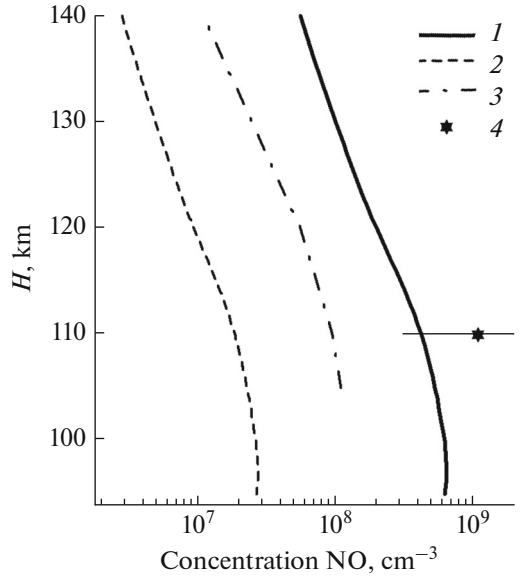

Fig. 8. Concentration of nitric oxide NO: (*1*) profile obtained in this model, (*2*) profile calculated for the 20-min interval, (*3*) profile obtained in [4] for the 20-min interval, (*4*) concentrations measured in [58] (horizontal line shows the measurement error).

noted that, according to the data of ground-based photometric measurements during the period of rocket flight, the intensity of the 391.4-nm emission of the auroral arc underwent no substantial variations for 20 min. This fact makes it possible to take the precipitating electrons flux to be constant in the period when rocket measurements were conducted.

Based on the experiment condition [3], integration using formula (2) was performed with the assumption that the electron precipitation lasts 20 min. The neutral atmosphere model was adapted to the observation conditions. The MSIS-90 [57] model was chosen as an initial neutral atmosphere model. Above 160 km, the N_2, O_2, and O concentrations were adjusted to the concentrations of these gases measured in the experiment. Below 160 km, the concentrations of molecular and atomic oxygen were corrected to obtain the best agreement between the calculated and experimental concentrations of the corresponding ions. Figure 6 shows the vertical profiles of concentrations of N_2, O_2, and O used in the calculations. The spectrum reconstructed from the vertical profile of the 391.4 nm emission measured in the experiment using the procedure described above was used as an initial electron spectrum. The pitch-angle distribution was taken to be isotropic over the lower hemisphere, this fact corresponding to the experimental data [3].

Figure 7 shows the calculated time dynamics of the concentration of the N_2^+, O_2^+, O^+, and NO^+ ions and the emission intensity in the 391.4, 320.0, 337.1, 557.7, and 630.0 nm lines. Figure 7 shows that a 20-min interval is sufficient for ion concentrations and emission intensity to reach a stationary state. For nitric oxide NO, the time of reaching a stationary state, as well as its lifetime after the end of precipitation, is a few days. In publication [58], which is dedicated to studies of the NO_2 continuum, the authors estimated the nitric oxide concentration for the day of the experiment equal to 1.1×10^9 cm^{-3} at a height of 110 km. This amount of NO molecules could not be achieved for 20 min. That is why the profile of NO obtained from the profile calculated for the 20-min interval by its normalizing based on minimization of deviations of calculated concentrations of all ions and emission intensities from the values obtained in the experiment was used in the model calculations. That profile is shown in Fig. 8 by solid curve. The NO concentration peak is obtained equal to 6×10^8 cm^{-3} at a height of 105 km. At a height of 110 km, the obtained value lies within the errors in [58]. The same figure shows the profiles obtained over the 20-min interval in this paper and in [4]. Neither one nor the other profile satisfies the estimates in [58], and such amount of nitric oxide cannot be sufficient to obtain for the ion concentrations measured in the experiment.

Figures 9 and 10 show the height profiles of the concentrations of the N_2^+, O_2^+, O^+, and NO^+ ions and the electron concentration and the height profiles of the intensity of the 557.7, 630.0, 391.4, 337.1, and

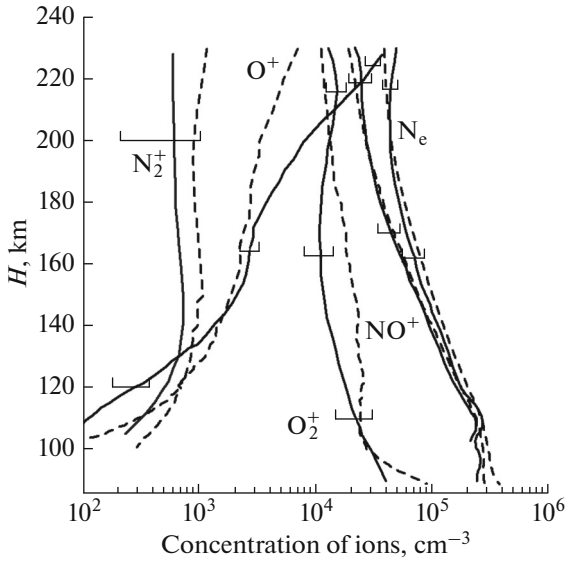

Fig. 9. Vertical profiles of the concentration of the N_2^+, O_2^+, O^+, and NO^+ ions and electrons: dashed curves show modeling results and solid curves show experimental data [4]. Horizontal lines show the measurements errors.

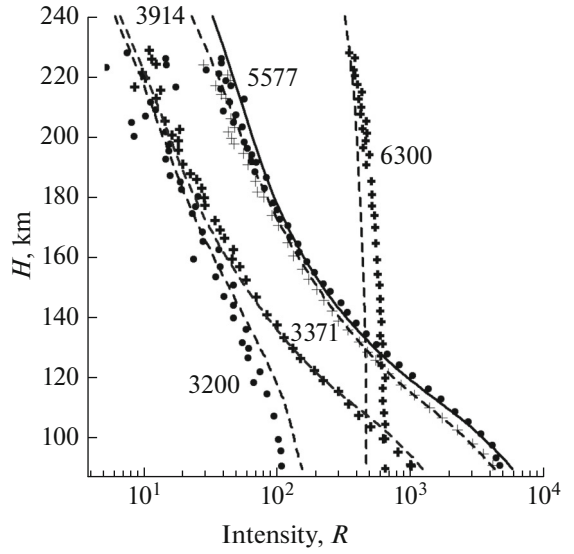

Fig. 10. Vertical profiles of the 557.7-, 630.0-, 391.4-, 337.1-, and 320.0-nm emission intensities: curves shows the modeling results, circles and crosses show experimental data [4].

320.0 nm emissions calculated by the model under consideration and measured in the experiment. For the sake of comparison, Fig. 11 shows the height distribution of the ratios of the measured concentrations of N_2^+, O_2^+, O^+, NO^+, and n_e, as well as ratios of the measured intensities of the emissions 391.4, 320.0, 337.1, 557.7, and 630.0 nm to the corresponding values calculated using the given model. Horizontal lines show the errors in measurements of ion concentrations and intensities. The error for an intensity of 320.0 nm emission and for the rest of the emissions is approximately 35 and 30%, respectively. It can be seen that, in the majority of cases, the ratios of the model and experimental values lie within the measurement errors and, in some cases, oscillate around unity. Thus, the model presented here correctly describes the processes in the Earth's upper atmosphere under the conditions of aurorae.

5. CONCLUSIONS

A numerical model describing processes of interaction of the main excited and ionized atmospheric constituents during auroral electron precipitations is presented in this paper. The model is based on the data available in scientific publications and contains 56 physicochemical reactions, rate constants of which are taken with allowance for recent measurements. Moreover, in order to correctly calculate the intensity of the emissions of the molecular nitrogen band systems, physicochemical reactions that describe the energy redistribution between vibrational levels of the N_2 triplet states are included in the model.

The method of calculating vertical profiles of the atmospheric gases excitation rates into the basis of which a functional that makes it possible to analytically relate the vertical profiles of excited constituents of the atmosphere into the energy spectrum of precipitating electrons is a distinctive feature of the model. The numerical model makes it possible to calculate vertical profiles of 14 ionospheric constituents, including electrons; time dynamics of the ionospheric constituent concentrations and vertical profiles of the intensity of the main auroral emissions including 557.7 and 630.0 nm; and emissions of the first negative, second positive, and Vegard–Kaplan band systems.

The presented model was approbated using the data of a unique coordinated rocket–satellite experiment in which the following parameters were measured: the energy spectrum of auroral electrons; concentrations of the atmospheric gases N_2, O_2, and O within a height interval of 160–240 km; vertical profiles of the N_2^+, O_2^+, O^+, and NO^+ ions; and vertical profiles of the intensities of emissions 557.7 and 630.0 nm of atomic oxygen, 391.4 nm of the first negative N_2^+ band system, 337.1 nm of the second positive band system, and 320.0 nm of the Vegard–Kaplan band system. A comparison of the calculated and experimental data shows that the presented model well describes the processes in the Earth's upper atmosphere under the auroral conditions and is currently the best possible

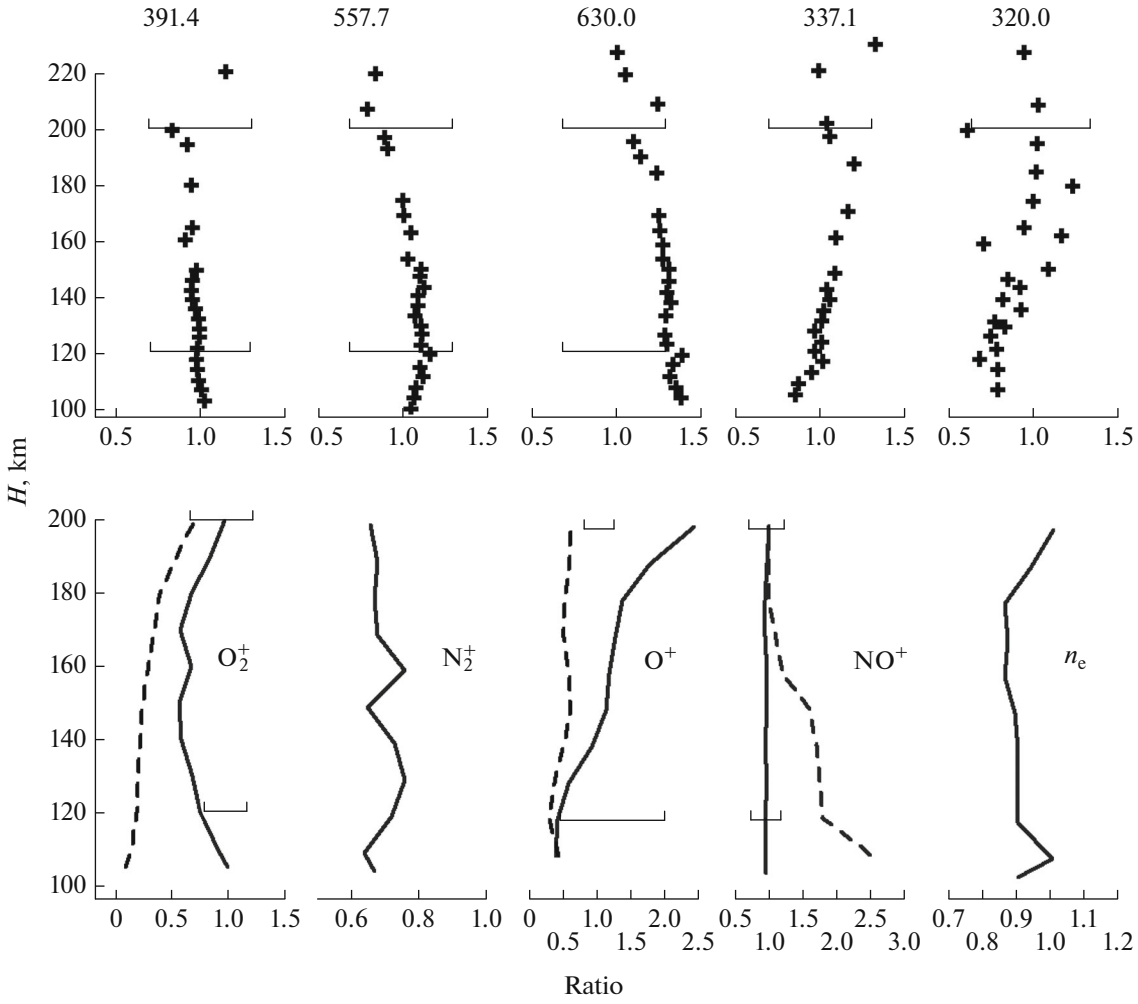

Fig. 11. Vertical distribution of the ratios of measured and calculated values. Dashed curves show the results of [4], horizontal lines show the measurements error.

way obtain mutual agreement with the values measured in the experiment.

REFERENCES

1. Jones, R.A. and Rees, M.H., Time dependent studies of the aurora —1. Ion density and composition, *Planet. Space Sci.*, 1973, vol. 21, no. 4, pp. 537–557.
2. Rees, M.H. and Jones, R.A., Time dependent studies of the aurora—2. Spectroscopic morphology, *Planet. Space Sci.*, 1973, vol. 21, no. 7, pp. 1213–1235.
3. Rees, M.H., Stewart, A.I., Sharp, W.E., et al., Coordinated rocket and satellite measurements of an auroral event. 1. Satellite observation and analysis, *J. Geophys. Res.*, 1977, vol. 82, no. 16, pp. 2250–2261.
4. Sharp, W.E., Rees, M.H., and Stewart, A.I., Co-ordinated rocket and satellite measurements of an auroral events. 2. The rocket observations and analysis, *J. Geophys. Res.*, 1979, vol. 84, no. A5, pp. 1977–1985.
5. Gerard, J.-C. and Rusch, D.W., The auroral ionosphere: Comparison of time-dependent model with composition measurements, *J. Geophys. Res.*, 1979, vol. 84, no. A8, pp. 4335–4340.
6. Ivanov, V.E. and Sergienko, T.I., *Vzaimodeistvie avroral'nykh elektronov s atmosfernymi gazami (statisticheskoe modelirovanie)* (Interaction of Auroral Electrons with Atmospheric Gases (Statistical Modeling)), St. Petersburg: Nauka, 1992.
7. Sergienko, T.I. and Ivanov, V.E., A new approach to calculate the excitation of atmospheric gases by auroral electron impact, *Ann. Geophys.*, 1993, vol. 11, no. 8, pp. 717–727.
8. Ivanov, V.E. and Kozelov, B.V., *Prokhozhdenie elektronnykh i protonno-vodorodnykh puchkov v atmosfere Zemli* (Propagation of Electron and Proton–Hydrogen Beams in the Earth's Atmosphere), Apatity: Kol'skii nauchnyi tsentr RAN, 2001.
9. Lindinger, W., Fehsenfeld, F.C., Schmeltekopf, A.L., et al., Temperature dependence of some ionospheric ion-neutral reactions from 300 to 900 K, *J. Geophys. Res.*, 1974, vol. 79, no. 31, pp. 4753–4756.
10. McFarland, M., Albritton, D.L., Fehsenfeld, F.C., et al., Energy dependence and branching ratio of the

N_2^+ + O reaction, *J. Geophys. Res.*, 1974, vol. 79, no. 19, pp. 2925–2926.

11. Fehsenfeld, F.C., Dunkin, D.B., and Ferguson, E.E., Rate constant for the reactions of with O, O_2 and NO; N_2^+ with O and NO; and O_2^+ with NO, *Planet. Space Sci.*, 1970, vol. 18, no. 8, pp. 1267–1270.
12. Mul, P.M. and McGowan, J.W., Merged electron–ion beam experiments. III. Temperature dependence of dissociative recombination of atmospheric ions NO^+, O_2^+ and N_2^+, *J. Phys. B*, 1979, vol. 12, pp. 1591–1602.
13. Queffelec, J.L., Rowe, B.R., Morlais, M., et al., The dissociative recombination of N_2^+ ($v = 0.1$) as source of metastable atoms in planetary atmosphere, *Planet. Space Sci.*, 1985, vol. 33, no. 3, pp. 263–270.
14. Abreu, V.J., Solomon, S.C., Sharp, W.E., et al., The dissociative recombination of the quantum yield of $O(^1S)$ and $O(^1D)$, *J. Geophys. Res.*, 1983, vol. 88, no. A5, pp. 4140–4144.
15. Fehsenfeld, F.C., The reaction of O_2^+ with atomic nitrogen and $NO^+ \cdot H_2O$ and NO_2^+ with atomic oxygen, *Planet. Space Sci.*, 1977, vol. 25, no. 2, pp. 195–196.
16. Kopp, J.P., Rusch, P.W., Roble, R.G., et al., Photoemission in the second position system of molecular nitrogen in the Earth's dayglow, *J. Geophys. Res.*, 1977, vol. 82, no. 4, pp. 555–560.
17. Lindinger, W. and Ferguson, E.E., Laboratory investigation of the ionospheric O_2^+ ($X^2\Pi_g$, $v = 0$) reaction with NO, *Planet. Space Sci.*, 1983, vol. 31, no. 10, pp. 1181–1182.
18. Goldan, P.D., Schmeltekopf, A.L., Fehsenfeld, F.C., et al., Thermal energy ion-neutral reaction rates. II. Some reactions of ionospheric interest, *J. Chem. Phys.*, 1966, vol. 44, no. 11, pp. 4095–4103.
19. St-Mourice, J.-P. and Torr, D.G., Nonthermal rate coefficients in the ionosphere: The reaction of O^+ with N_2, O_2 and NO, *J. Geophys. Res.*, 1978, vol. 83, no. A3, pp. 969–977.
20. Johnsen, R. and Biondi, M.A., Laboratory measurement of the $O^+(^2D) + N_2$ and $O^+(^2D) + O_2$ reaction rate coefficients and their ionospheric implications, *Geophys. Res. Lett.*, 1980, vol. 7, no. 5, pp. 401–403.
21. Torr, D.G. and Torr, M.R., Chemistry of the thermosphere and ionosphere, *J. Atmos. Terr. Phys.*, 1979, vol. 41, nos. 7/8, pp. 797–839.
22. Prandhan, A.K., Close-coupling calculations for electron collisions with O^+ and for bound states of neutral oxygen, *J. Phys. B: At. Mol. Phys.*, 1976, vol. 9, no. 3, pp. 433–443.
23. Kernahan, J.H. and Pang, H.L., Experimental determination of absolute *A* coefficients for 'forbidden' atomic oxygen lines, *Can. J. Phys.*, 1975, vol. 53, no. 5, pp. 455–458.
24. Oppenheimer, M., Constantinides, E.R., Kirby-Docken, K., et al., Ion photochemistry of the thermosphere from Atmospheric Explorer-C measurements, *J. Geophys. Res.*, 1977, vol. 82, no. 35, pp. 5485–5492.
25. Rusch, D.W., Torr, D.G., Hays, P.B., et al., The OII (7319–7330 Å) dayglow, *J. Geophys. Res.*, 1977, vol. 82, no. 4, pp. 719–722.
26. Solomon, S.C., Hays, P.B., and Abreu, V.J., The auroral 6300 Å emission: Observations and modeling, *J. Geophys. Res.*, 1988, vol. 93, no. A9, pp. 9867–9882.
27. Wiese, W.L., Smith, M.W., and Glennon, B.M., *Atomic Transition Probabilities*, vol. 1, Washington, D.C.: National Bureau of Standards, 1966.
28. Seaton, M.J. and Osterbrock, D.E., Relative OII intensities in gaseous nebulae, *Astrophys. J.*, 1957, vol. 125, pp. 66–82.
29. Henry, R.J., Burke, P.G., and Sinfailam, A.-L., Scattering of electrons by C, N, O, N^+, O^+ and O^{++}, *Phys. Rev.*, 1969, vol. 178, no. 1, pp. 218–225.
30. Streit, G.E., Howard, C.J., Schmeltekopf, A.L., et al., Temperature dependence of $O(^1D)$ rate constants for reactions with O_2, N_2, CO_2, O_3, and H_2O, *J. Chem. Phys.*, 1976, vol. 65, no. 11, pp. 4761–4764.
31. Abreu, V.J., Yee, J.H., Solomon, S.C., et al., The quenching rate of $O(^1D)$ by $O(^3P)$, *Planet. Space Sci.*, 1986, vol. 34, no. 11, pp. 1143–1146.
32. Fisher, C.F. and Saha, H.P., Multiconfiguration Hartree–Fock results with Breit–Pauli corrections for forbidden transitions in the $2p^4$ configuration, *Phys. Rev. A*, 1983, vol. 28, no. 6, pp. 3169–3178.
33. Berrington, K.A. and Burke, P.G., Effective collision strengths for forbidden transitions in e-N and e-O scattering, *Planet. Space Sci.*, 1981, vol. 29, no. 3, pp. 377–380.
34. Slander, T.G. and Black, G., Quenching of $O(^1S)$ by $O_2(a^1\Delta g)$, *Geophys. Res. Lett.*, 1981, vol. 8, no. 5, pp. 535–538.
35. Slander, T.G. and Black, G., $O(^1S)$ quenching profile between 75 and 115 km, *Planet. Space Sci.*, 1973, vol. 21, no. 10, pp. 1757–1762.
36. Black, G., Slander, T.G., St. John, G.A., et al., Vacuum-ultraviolet photolysis of N_2O. IV. Deactivation of $N(^2D)$, *J. Chem. Phys.*, 1969, vol. 51, no. 1, pp. 116–121.
37. De More, W.B., Sander, S.P., Golden, D.M., et al., *Chemical Kinetics and Photochemical Data for Use in Stratospheric Modeling* (*Evaluation Number 9, JPL Publication 90-1)*, Pasadena, CA: Jet Propulsion Laboratory, California Institute of Technology, 1990.
38. Gerard, J.-C., Thermospheric odd nitrogen, *Planet. Space Sci.*, 1992, vol. 40, nos. 2/3, pp. 337–353.
39. Lin, C.-L. and Kaufman, F., Reactions of metastable nitrogen atoms, *J. Chem. Phys.*, 1971, vol. 55, no. 8, pp. 3760–3769.
40. Link, R., A rocket observation of 6300 Å /5200 Å intensity ratio in the dayside aurora: Implications for the production of $O(^1D)$ via the reaction $N(^2D) + O^2 \rightarrow NO + O(^1D)$, *Geophys. Res. Lett.*, 1983, vol. 10, no. 3, pp. 225–228.
41. Fell, C., Steinfeld, J.I., and Miller, S., Quenching of $N(^2D)$ by $O(^3P)$, *J. Chem. Phys.*, 1990, vol. 92, no. 8, pp. 4768–4777.
42. Schofield, K., Critically evaluated rate constants for gaseous reactions of several electronically excited species, *J. Phys. Chem. Ref. Data*, 1979, vol. 8, no. 3, pp. 723–798.

43. Frederick, J.E. and Rusch, D.W., On the chemistry of metastable atomic nitrogen in the *F* region deduced from simultaneous satellite measurement of the 5200-Å airglow and atmospheric composition, *J. Geophys. Res.*, 1977, vol. 82, no. 25, pp. 3509–3517.
44. Bates, D.R., Theoretical considerations regarding some inelastic atomic collision processes of interest in aeronomy: Deactivation and charge transfer, *Planet. Space Sci.*, 1989, vol. 37, no. 3, pp. 363–368.
45. Garstang, R.H., Transition probabilities in auroral lines, in *Airglow and Aurora*, New York: Pergamon, 1956, pp. 324–327.
46. Herron, J.T., Evaluated chemical kinetics data for reactions of $N(^2D)$, $N(^2P)$, and $N_2\left(A^3\Sigma_u^+\right)$ in the gas phase, *J. Phys. Chem. Ref. Data*, 1999, vol. 28, no. 5, pp. 1453–1483.
47. Kley, D., Lawrence, G.M., and Stone, E.J., The yield of $N(^2D)$ atoms in the dissociative recombination of NO^+, *J. Chem. Phys.*, 1977, vol. 66, no. 9, pp. 4157–4165.
48. Langford, A.O., Bierbaum, V.M., and Leone, S.R., Auroral implications of recent measurements on $O(^1S)$ and $O(^1D)$ formation in the reaction of N^+ with O_2, *Planet. Space Sci.*, 1985, vol. 33, no. 10, pp. 1225–1228.
49. Torr, M.R., The *N*II 2143 Å dayglow from Spacelab 1, *J. Geophys. Res.*, 1985, vol. 90, no. 7, pp. 6679–6684.
50. Kirillov, A.S. and Aladjev, G.A., The role of the $N_2\left(A^3\Sigma_u^+, v\right)$ + O reaction in the green line airglowand vibrational kinetics of molecular nitrogen in the high-latitude upper atmosphere, *Cosmic Res.*, 1998, vol. 36, no. 5, pp. 423–429.
51. Morrill, J.S. and Benesch, W.M., Auroral N_2 emissions and effect of collisional processes on N_2 state vibrational populations, *J. Geophys. Res.*, 1996, vol. 101, no. A1, pp. 261–274.
52. Gilmore, F.R., Laher, R.R., and Espy, P.J., Franck–Condon factors, *r*-centroids, electronic transition moments, and Einstein coefficients for many nitrogen and oxygen band systems, *J. Phys. Chem. Ref. Data*, 1992, vol. 21, no. 5, pp. 1005–1107.
53. Kirillov, A.S., The study of intermolecular energy transfers in electronic energy quenching for molecular collisions N_2–N_2, N_2–O_2, O_2–O_2, *Ann. Geophys.*, 2008, vol. 26, pp. 1149–1157.
54. Thomas, J.M. and Kaufman, F., Rate constants of the reactions of metastable $N_2\left(A^3\Sigma_u^+\right)$ in $v = 0$, 1, 2, and 3 with ground state O_2 and O, *J. Chem. Phys.*, 1985, vol. 83, no. 6, pp. 2900–2903.
55. Jones, R.A. and Gattinger, R.L., Quenching of the N_2 Vegard–Kaplan system in aurora, *J. Geophys. Res.*, 1976, vol. 81, no. 4, pp. 497–450.
56. Eastes, R.W. and Sharp, W.E., Rocket-borne spectroscopic measurements in the ultraviolet aurora: The Lyman–Birge–Hopfield bands, *J. Geophys. Res.*, 1987, vol. 92, no. A9, pp. 10095–10100.
57. MSIS-E-90 Atmosphere Model. http://omniweb.gsfc.nasa.gov/vitmo/msis_vitmo.html.
58. Sharp, W.E., NO_2 continuum in aurora, *J. Geophys. Res.*, 1978, vol. 83, pp. 4373–4376.

Translated by A. Danilov